Published in final edited form as:

J Neurochem. 2020 March ; 152(5): 585–601. doi:10.1111/jnc.14912.

Decreased levels of constitutive proteasomes in experimental autoimmune encephalomyelitis may be caused by a combination of subunit displacement and reduced *Nfe2l1* expression

Kara L. Shanley[*], **Che-Lin Hu**[*], **Oscar A. Bizzozero**

Dept. of Cell Biology and Physiology, University of New Mexico - Health Sciences Center, Albuquerque, New Mexico.

Abstract

The goal of this study was to determine if subunit displacement and/or alterations in proteasome biosynthesis could explain the changes observed in the levels of constitutive proteasomes (c-20S) and immunoproteasomes (i-20S) in the spinal cords of mice with experimental autoimmune encephalomyelitis (EAE). To this end, EAE was induced in C57BL/6 mice by immunization with $MOG_{35–55}$ peptide. Spinal cords were collected at different times during the disease course and used for western blotting, RNA analysis and immunohistochemistry. The results show that, as expression of i-20S and the activator PA28 rise in EAE, there is a concomitant decline in that of c-20S at the mRNA and protein level. These changes are observed in neurons and astrocytes but not oligodendrocytes. The increased amounts of the i-20S-specific subunit β5i and PA28α/β in EAE correlate with the levels of IFN-γ and its downstream effectors p-STAT-1 and IRF-1, but not with those of NF-κB. This suggests the STAT-1/IRF-1 pathway is solely responsible for the induction of these subunits. The decrease in the mRNA and protein levels corresponding to the c-20S-specific subunit β5 may also be due to reduced expression of the nuclear factor (erythroid-derived 2)-like-1 (Nrf1 or *Nfe2l1*), specifically Nrf1α and Nrf1β. Low *Nfe2l1* mRNA expression is unlikely caused by reduced mTOR signaling but could be the result of diminished pre-B-cell leukemia homeobox-1 transcription factor (PBX1) levels. Together, these findings suggest that a combination of subunit displacement and reduced Nrf1 expression may be responsible for c-20S impairment in EAE. The present work provides insights into the dynamics of proteasome expression in the CNS of EAE mice and is the first to explore Nrf1 signaling in an inflammatory demyelinating disorder.

Graphical Abstract

Correspondence should be addressed to: Dr. Oscar A. Bizzozero, Department of Cell Biology and Physiology, University of New Mexico School of Medicine, 1 University of New Mexico, MSC08 4750, Albuquerque, NM 87131, Tel: (505) 272-5520, FAX: (505) 272-9105, obizzozero@salud.unm.edu.

[*]These authors contributed equally to this work.

Disclosure/conflict of interest

The authors have no conflict of interest.

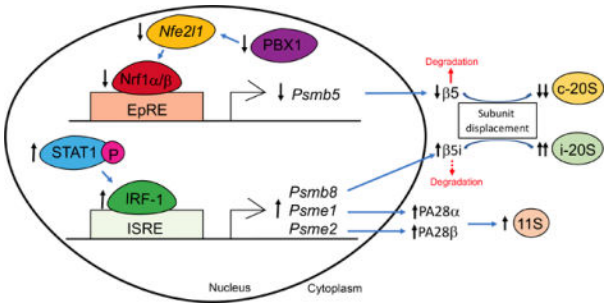

Proteasome composition in experimental autoimmune encephalomyelitis (EAE) is determined by a number of signaling pathways. Here, we show that the number of immunoproteasomes is increased in neurons and astrocytes from mice EAE spinal cords at the peak of the disease and is probably due to a rise in phosphorylated signal transducer and activator of transcription 1 (p-STAT1) and interferon regulatory factor-1 (IRF-1) levels. Immunoproteasome overexpression is accompanied by a decrease in constitutive proteasomes levels, which correlates with low expression of nuclear factor (erythroid-derived 2)-like 1 (Nrf1) and is likely caused by reduced pre-B-cell leukemia homeobox-1 transcription factor (PBX1) signaling. The displacement of constitutive subunits by their inducible counterparts may also be responsible for alterations in proteasome composition. The present work provides insights into the dynamics of proteasome expression in EAE and is the first to explore Nrf1 signaling in an inflammatory demyelinating disorder.

Keywords

inflammatory cytokines; experimental autoimmune encephalomyelitis; immunoproteasome; multiple sclerosis; Nrf1; PA28; proteasome; STAT-1 signaling

Introduction

Proteasomes are multi-enzyme complexes whose sole function is to catalyze the degradation of most intracellular proteins. Thus, these particles play critical roles in signaling mechanisms, cell function and cellular homeostasis (Rechsteiner and Hill, 2005). The core of these complexes, the 20S proteasome, is comprised of two outer α and two inner β rings (i.e. αββα). Each α and β rings are made of seven α subunits (α1-α7) and seven β subunits (β1-β7), respectively (Ethen *et al.* 2007). While the α rings are the structural components of the proteasome, each β ring has three proteolytic sites, which display caspase-like (β1), trypsin-like (β2) and chymotrypsin-like (β5) activities (Coux *et al.* 1996). The expression, structure and activity of proteasomes are regulated tightly and are constantly adjusted by to fulfill cellular requirements. For example, exposure of cells to cytokines, such as interferon-γ (IFN-γ), leads to the replacement of the catalytic β1, β2 and β5 subunits in the constitutive 20S particle (c-20S) by the inducible β1i, β2i and β5i subunits, forming the immunoproteasome 20S particle (i-20S) (Aki *et al.* 1994). Immunoproteasomes were initially thought to be present only in immune cells, where they participate in the generation of peptides for antigen presentation. However, recent studies have shown that i-20S particles are expressed in most tissues and play roles that are unrelated to the immune system (Seifert

et al. 2010; Hussong *et al*. 2010). Proteasome activity is regulated by a number of protein complexes that attach to one or both ends of the αββα barrel. One of these regulators is PA28 (11S), also induced by IFN-γ, which attaches to the i-20S particle forming a complex (11S/i-20S/11S). This complex produces more peptides of the correct length for the major histocompatibility complex class 1 antigen processing (Rivett and Hearn, 2004). PA700 (19S), the other major activator, binds to one or both ends of the 20S core particle to form the 26S and 30S proteasome, respectively. These complexes recognize and hydrolyze abnormal and misfolded proteins conjugated with polyubiquitin chains (Braun *et al*., 1999).

While little is known about how proteasome and immunoproteasome expression is controlled under basal conditions, more information is available on how levels of proteasomes are regulated under stress conditions. For example, IFN-γ augments the transcription of the immunoproteasome-specific β subunits (Aki *et al*., 1994) via binding of STAT-1-dependent interferon regulatory factor-1 (IRF-1) to IFN-γ regulatory elements in the promoter regions of these genes (Foss and Prydz, 1999). In cells containing both c-20S and i-20S particles, a rise in the content of inducible subunits is accompanied by a reduction in the amounts of constitutive subunits by a well characterized process known as subunit displacement (Früh *et al*., 1994). In addition to post-translational downregulation of constitutive proteasomes in inflammatory conditions, the promoter regions of the genes that encode for the constitutive proteasome subunits and the 11S and 19S activators have electrophile response elements (EpRE) that bind nuclear factor–erythroid-2–related factors (Pickering *et al*., 2012) These proteins belong to the cap'n'collar subfamily of basic-region leucine zipper transcription factors, and include Nrf1 (*Nfe2l1*), Nrf2 (*Nfe2l2*), Nrf3 (*Nfe2l3*) and the p45 subunit (Motohashi *et al*., 2002). Both Nrf1 and Nrf2 form heterodimers with small Maf proteins that bind to EpRE and activate transcription (Venugopal and Jaiswal 1998; Biswas and Chan 2010). The amount of Nrf1 augments upon endoplasmic reticulum stress and mild proteasome inhibition by a post-translational mechanism (Bugno *et al*., 2015; Xiang *et al*., 2018), whereas Nrf2 levels increase following oxidative stress (Kobayashi *et al*., 2004). While both transcription factors have the potential to increase proteasome subunit expression, Nrf1 alone is required for the upregulation of proteasome genes in response to proteasome inhibition (Radhakrishnan *et al*., 2010). Additionally, Nrf1 deletion in neuronal cells causes proteasome impairment due to down-regulation of proteasomal genes that encode the catalytic subunits (Lee *et al*., 2011). Thus, Nrf1 seems to be more important than Nrf2 for promoting constitutive proteasome synthesis.

Experimental autoimmune encephalomyelitis (EAE) is a well-established animal model for CNS autoimmune disorder, recapitulating a number of clinical and pathological features of multiple sclerosis (MS) (Gold *et al*., 2000). Several EAE models exist that mimic the different clinical courses of MS. $MOG_{35–55}$ peptide-induced EAE in the C57BL/6 mouse, the animal model used in this study, is characterized by the presence of inflammatory lesions in the CNS that are present mostly in the spinal cord and the cerebellum (Kuerten *et al*., 2007). Our laboratory was the first to demonstrate that the peptidase activity of the proteasome is altered in MS brains (Zheng and Bizzozero, 2011) and EAE cerebella (Zheng and Bizzozero, 2010). Furthermore, we discovered that the changes in the levels of the three catalytic subunits of c-20S and i-20S proteasomes account for all the fluctuations of proteasomal peptidase activities during the disease course of EAE (Zheng *et al*., 2012). The

goal of the present study was to determine if subunit displacement and/or alterations in proteasome biosynthesis could explain the changes in the levels of proteasomes and their activators observed in the spinal cords of EAE animals during the inflammatory phase. The results show that, as expression of i-20S and PA28 rise in EAE, there is a concomitant decline in that of c-20S at the mRNA and protein level. Interestingly, these changes are observed in neurons and astrocytes but not oligodendrocytes. The increase in the amount of the i-20S-specific subunit β5i and PA28α/β in EAE correlate with the levels of IFN-γ and its downstream effectors STAT-1 and IRF-1. Finally, we show that the decrease in the c-20S-specific subunit β5 mRNA levels may also be due to reduced Nrf1 expression. Together, these findings suggest that a combination of subunit displacement and reduced Nrf1 expression may be responsible for c-20S impairment in EAE. The present work provides insights into the dynamics of proteasome expression in the CNS of EAE mice and is the first to explore Nrf1 signaling in an inflammatory demyelinating disorder.

Materials and Methods

Preparation of EAE animals and tissue collection

Housing and all procedures of the animals were in strict accordance with the NIH Guide for the Care and Use of Laboratory Animals, and approved by the Institutional Animal Care and Use Committee (protocol #16–200424-HSC). Adult female C57Bl/6 mice (8-week old) were purchased from Envigo (MGI:2161078, previously Harlan Laboratories, Indianapolis, IN). Three to four arriving mice were arbitrarily placed in standard ventilated cages for one week of habituation before EAE induction. No randomization was performed to assign the cages to control or the EAE group. All mice housed in the same cage received the same inoculation. This is necessary because the weaker (EAE) mice could have trouble competing against healthy (control) mice for accessibility to food and water. To induce EAE, mice (~20 g of body weight) received a subcutaneous injection (200 μl) into the lower back area of custom synthesized $MOG_{35–55}$ peptide (200 μg) (21^{st} Century Biochemicals; Marlborough, MA) in saline mixed with complete Freund's adjuvant (CFA) (1:1) constaining of 4 mg/ml of heat killed Mycobacterium tuberculosis H37Ra (cat #7001; Chondrex Inc; Redmond, WA). Control mice received saline mixed with CFA without MOG peptide. Two and 48 h after EAE induction, all animals received an intraperitoneal injection of 0.3 μg of pertussis toxin (PTX, cat#180, List Biological Laboratories; Campbell, CA) in 100 μl of saline. Seven days after disease induction, mice received a second immunization on the other flank. This immunization protocol with 2 MOG peptide injections causes a persistent type of EAE, allowing to compare changes that occur in the acute (mostly inflammatory) and the chronic (mostly neurodegenerative) phase of the disease. Food and water were placed on the cage floor to ensure access to nourishment. No measures were taken to minimize possible pain after disease induction because analgesic and anti-inflammatory drugs may affect the disease course. Animals were weighed and examined daily for the presence of neurological signs. Normally, mice that experience a loss of 30% in body weight or have very severe symptoms (moribund stage) are euthanized and removed from the experiment. However, in this study no animal reached that stage and therefore no animal was excluded. A schematic timeline of the study design is depicted in Fig. 1. At various times during the course of the disease, 9 – 60 days post-immunization (dpi), EAE and CFA-injected controls were euthanized by

decapitation under inhaled anesthesia of isoflurane (2–3% cat# 430024079, Piramal Critical Care Inc; La Vergne, TN). The spinal cords were removed using the hydraulic extrusion method. The excised cervical and thoracic sections were flash-frozen for RNA extraction or immediately homogenized in 20 mM sodium phosphate buffer pH 7.5 containing 1 mM EDTA, 0.1 mM neocuproine, 2 mM 4,5 dihydroxy-1,3 benzene disulfonic acid, 1 mM dithiothreitol (DTT), 1× cOmplete™ protease inhibitor cocktail (cat#11873580001; Sigma; St Louis, MO) and 1× PhosSTOP™ phosphatase inhibitor (cat#04906845001; Sigma). Protein homogenates were stored at −80°C until use. Protein concentration was determined with Bradford-based chemistry using Bio-Rad protein assay dye reagent (cat#5000006; Bio-Rad Laboratories; Hercules, CA) with bovine serum albumin as a standard. Lumbar spinal cord sections were used for histological (hematoxylin and eosin staining) and immunofluorescence analysis (see below). This region has more lesions than other spinal cord areas making the pathological changes easy to assess. It is important to note that blinding was not done from the beginning of the study due to the fact that EAE mice exhibit neurological symptoms and thus can be easily identified. However, tissue samples (RNA, protein lysates and histological sections) were assigned with new serial numbers during all experimental procedures. Sample IDs were only revealed to the investigator after data acquisition. This study was not pre-registered.

Subcellular fractionation

Preparation of the crude nuclear fraction was carried out using a modified nuclear extraction protocol adapted from Thermo-Fisher Scientific. Briefly, small spinal cord sections were homogenized at 4°C in 0.5 ml of hypotonic buffer solution (20 mM Tris-HCl pH 7.4 containing 10 mM NaCl, 3 mM $MgCl_2$, 1 mM DTT, 1 mM phenylmethylsulphonyl fluoride and 1× protease inhibitor cocktail) using a glass/teflon Dounce tissue homogenizer (20 up/down strokes). Suspensions were kept on ice for 15 min, mixed with 25 µl of 10% w/v Nonidet P-40 and centrifuged at 3,000 *g* for 10 min. The supernatant (cytosolic fraction) and the pellet (crude nuclear fraction) were collected, and proteins were solubilized in sodium dodecyl sulfate (SDS) sample buffer and analyzed by western blotting.

Reverse transcription and qPCR

Snap-frozen spinal cord tissue were homogenized in Trizol® (cat#15596026, Invitrogen; Carlsbad, CA) reagent and total RNA extracted following manufacturer's protocol. Complementary DNA (cDNA) was prepared from DNase I-treated total RNA and synthesized using the SuperScript II First-Strand Synthesis system (cat#18064022, Invitrogen). Quantitative RT-PCR was conducted on the Applied Biosystems 7500 Fast Real-Time PCR System by mixing 20 ng cDNA with 1 µM of gene-specific primers (Table 1) and amplified with the Power SYBR Green PCR MasterMix (cat#4367659, Applied Biosystems, Forster City, CA) using a preset program (50°C for 10 min, 95°C for 10 min and then 40 cycles of 95°C/15 sec and 60°C/1 min). The relative mRNA expression levels for the genes of interest were determined using the comparative $2^{-\Delta Ct}$ method (Livak and Schmittgen 2001) by normalizing the Ct values of target genes to the geometric mean Ct of 4 house-keeping genes (*Gapdh*, *Hprt1*, *Rplp0* and *Rn18s*) (Table 1) (Vandesompele *et al.* 2002). In all cases, the normalized values from EAE mice were expressed as relative to the average from control animals. The variations of control values are shown in the figures.

Western blot analysis

Proteins (5 μg) were separated by SDS–polyacrylamide gel electrophoresis on 4–20% Mini-Protean TGX gels (cat#4561096; Bio-Rad Laboratories; Hercules, CA) and were blotted to polyvinylidene difluoride membranes. Blots were blocked with 3% (w/v) non-fat milk in phosphate-buffered saline solution containing 0.05% (v/v) Tween 20 (PBS-T) and then incubated overnight at 4°C with the primary antibodies listed in Table 2. Membranes were rinsed three times in PBS-T and were incubated for 1 h with the corresponding horseradish peroxidase-conjugated secondary antibodies (Table 2). Blots were developed by enhanced chemiluminescence using the Western Lightning ECL™ kit (cat#NEL103; Perkin-Elmer, Boston, MA) and signals captured on blue X-ray films. Films were scanned in a Hewlett Packard Scanjet 4050 and the images were quantified using the NIH Fiji ImageJ 1.52 imaging analysis program (RRID:SCR_003070). Band intensities were normalized by the intensity of the Coomassie blue stain in the respective lanes or, in the case of the nuclear fractions, by the amount of histone H3. All the antibodies used in this study were validated by the suppliers and detected bands at the predicted molecular weights on western blots.

Immunofluorescence localization of proteasomes and immunoproteasomes

To assess cellular distribution of c-20S, i-20S and 11S particles in the lumbar spinal cords of control and EAE mice, we performed double-label immunofluorescence analyses using antibodies against β5, β5i, PA28β and various cell-specific markers on paraformaldehyde-fixed and paraffin-embedded sections. All the antibodies used for immunohistochemistry are listed in Table 3. Briefly, 5 μm-thick sections mounted to slides were deparaffinized and hydrated in down-grade alcohol series. Antigen retrieval was performed in 10 mM sodium citrate buffer (pH 6.0) with 0.05% Tween-20 using a heat-induced retrieval method. Spinal cord sections were blocked in 4% normal goat serum and then incubated with the primary antibodies at 4°C overnight. The various cell types were detected using mouse monoclonal antibodies against GFAP (glial fibrillary acidic protein) for astrocytes, CA-II (carbonic anhydrase-II) for oligodendrocytes, NeuN (neuronal nuclear antigen) for neurons and CD45 (cluster of differentiation 45) for leukocytes (Table 3). Target proteins and cell-specific markers were co-visualized with secondary antibodies conjugated to either a Cy™ 3 fluorophore or an Alexa Fluor® 488 that detect the respective antibody species (Table 3). Immunofluorescence images were captured with a Leica TCS SP5 confocal microscope system (Leica Microsystems Inc, Buffalo Grove, IL). Relative fluorescence of β5 and β5i immunoreactivity was quantified with the Leica Application Suite X (RRID:SCR_013673) using the histogram tool. To quantify the relative expression level on the fluorescence-labeled confocal images, individual regions of interest were delineated (hand draw tool) in the green, neural marker-labeled cells and returning the mean grey values in the red (β5 and β5i) channel. For each animal, a total of 8 confocal images from each stained slide (5–50 labeled cells/field) selected at random were analyzed. Values were expressed as the average fluorescence. Data for oligodendrocytes and astrocytes come from both white matter and gray matter. Data for neurons derive from gray matter and also include motor neurons.

Statistical Analysis

A minimum of 6 control and 6 EAE mice in each study group (dpi) were determined by power analysis using G*Power 3.1 software (RRID:SCR_013726; Kiel University, Germany) and the following parameters: *t*-test (difference between two independent means), two-tail, effective size = 2.0, $\alpha = 0.05$ and a power $(1-\beta) = 0.8$. The effective size was calculated assuming a difference between means of 20% and a SD = 0.10, which was taken from our previous study on proteasome composition in the cerebellum of EAE mice (Zheng *et al.*, 2012). Results were analyzed for statistical significance with the unpaired Student's *t*-test utilizing the GraphPad Prism® program 8.1 (RRID:SCR_002798; GraphPad Software Inc.; San Diego, CA) after assessing the normality of the data with the Shapiro-Wilk test. For data that did not follow a normal distribution, statistical significance was determined with the nonparametric Mann-Whitney test. Outliers in the data sets were identified using the GraphPad Prism® ROUT test and assigning a Q value of 1%, and were removed before the final statistical analysis.

Results

Pro-inflammatory cytokine expression and oxidative stress are elevated in EAE spinal cords.

EAE was induced in female C57BL/6 mice by double immunization with $MOG_{35–55}$ peptide as explained in "Materials and Methods" and shown in Fig. 1. Symptoms were graded according to the following scale: 0, no symptoms; 1, tail weakness; 1.5, clumsy gait; 2, hind limb paresis; 2.5, partial hind limb dragging; 3, hind limb paralysis; 3.5, hind limb paralysis with fore limb paresis; 4, complete paralysis; and 5, moribund. Neurological symptoms and spinal cord pathology start at 14 dpi (7 days after the second injection with MOG peptide), reaching a maximum after 21 dpi (Fig. 2a). CFA-injected animals (i.e. controls) do not present any neurological sign or spinal cord damage. In this study, we used a total of 26 control mice and 32 EAE mice. Except for the small sample size at 60 dpi (n = 3), the number of mice in each of the other control and EAE groups ranged between 5 and 8 (Fig. 1). This number is very close to the minimum of 6 mice per group predetermined by power analysis using the parameters described in "Materials and Methods".

As shown in Fig. 2b, lymphocyte infiltration in the spinal cord (as detected by staining the sections with hematoxylin and eosin) begins at 14 dpi reaching a maximum at 21 dpi. In contrast, IFN-γ mRNA expression in EAE is already high at 9 dpi (Fig. 2c) and remains elevated throughout the course of the illness. TNF-α mRNA levels in EAE are significantly elevated at 21 dpi and thereafter (Fig. 2d), while the temporal expression pattern of IL-1β mRNA is similar to that of IFN-γ, except for the values at 9 dpi (Fig. 2e). Glutathione levels in the diseased spinal cord decline progressively starting at 21 dpi (Fig. 2f). Overall, these data indicate the presence of significant inflammation and oxidative stress in the spinal cords of EAE mice, which are expected to upregulate immunoproteasome and constitutive proteasome expression, respectively.

Reduced c-20S and increased i-20S expression in EAE spinal cords

We next measured the mRNA expression of the immunoproteasome-specific subunit β5i (*Psmb8*) as well as that of PA28β (*Psme2*), a component of the 11S activator, in the spinal cord during the course of EAE (9 – 60 dpi). As expected from the temporal mRNA expression pattern of IFN-γ, TNF-α and IL-1β in EAE (Fig. 2c–e), *Psmb8 and Psme2* mRNA levels in the affected spinal cords become significantly higher than those in controls at 14 dpi, reaching a maximum between 21 dpi and 30 dpi to decrease thereafter (Fig. 3a,b). Similar results were obtained for PA28α (*Psme1*) (data not shown). In contrast, the constitutive proteasome-specific subunit β5 (*Psmb5*) mRNA expression diminishes in EAE starting already at 9 dpi, with the difference being maximal at 14 dpi - 21 dpi and declining after that period (Fig. 3c). Reduced β5 gene expression in EAE was an unexpected finding since constitutive proteasomes are known to be induced by oxidative stress, which is clearly demonstrated by the low glutathione levels in this disorder (Fig. 2f).

The amounts of proteasomes and their activators in EAE mice at 30 dpi, measured by western blot analysis of spinal cord proteins, is shown in Fig. 4a. The levels of proteasome core particles (c-20S + i-20S), assessed with an antibody that recognizes six of the seven 20S α-subunits (α1–3/5–7), increases in EAE by 75.7 ± 15.0% ($p = 0.0043$). However, α7-subunit (*Psma7*) mRNA expression is unchanged in EAE (Fig. 4b), suggesting the occurrence of translational and/or post-translational control mechanisms. Proteasome β5i, PA28α and PA28β proteins are greatly augmented in EAE (Fig. 4a), which agrees with their increased gene expression (Fig. 4b). The amount of the β5 subunit is reduced by 36.7 ± 7.8% ($p = 0.0007$) in EAE, which follows the 38% decrease in mRNA expression. Levels of the 19S-specific Rpt5 subunit rise by 107 ± 41% ($p = 0.0260$) while there is an 18% reduction in its mRNA levels (*Psmc3*).

Using the intensity values obtained by western blot analysis and purified c-20S and i-20S proteasomes for calibration, we estimated the absolute amounts of each proteasome core particle in control and EAE spinal cord homogenates. The purity of the the c-20S particle (positive for β1, β2 and β5 but not for their inducible counterparts) and the i-20S (positive for β1i, β2i and β5i but not for their standard counterparts) was demonstrated by western blotting in our previous publication (Zheng *et al.*, 2012). We found that in control spinal cords, ~86% of core particles correspond to c-20S proteasome (4.67 pmol/mg protein) and the rest (~14%) to the i-20S proteasome (0.73 pmol/mg protein). In contrast, only 33% of the proteasomes in EAE spinal cords at 30 dpi corresponds to the constitutive form (2.98 pmol/mg protein) while 67% (6.10 pmol/mg protein) was in the form of immunoproteasomes. Based on these numbers, the total amount of proteasomes (i.e. c-20S + i-20S) in EAE rises by 68%, which is close to the 75.7% increase observed by western blot analysis using the α1–3/5–7 antibody (Fig. 4a).

Neurons and astrocytes display altered levels of constitutive- and immuno-proteasomes

To ascertain whether the decrease in constitutive proteasome levels in EAE takes place in all spinal cord cells or whether it is limited to a particular cell type (neurons, astrocytes or oligodendrocytes), we conducted a double-label immunofluorescence confocal microscopy analysis. As shown in Fig. 5, images from control and EAE spinal cords at 30 dpi reveal the

presence of the c-20S-specific subunit β5 in the cytoplasm of all three major cell types. Staining was more intense in neurons (average intensity = 41) followed by oligodendrocytes (average intensity = 25) and astrocytes (average intensity = 18). Quantification of the images shows that β5 subunit labeling in EAE decreases by 47.0 ± 7.2 % ($p = 0.0014$) in neurons and by 54.1 ± 15.0% ($p = 0.0596$) in astrocytes, while levels of this subunit in oligodendrocytes are unchanged ($p = 0.3853$) (Fig. 7a). The reduced amount of β5 in neurons and astrocytes, along with the decreased number of oligodendrocytes in the EAE spinal cord (Hu *et al.*, 2019), is likely the reason for the 36.7% drop in β5 levels observed on western blots of total spinal cord proteins (Fig. 4a).

The average β5i intensity for neurons, astrocytes and oligodendrocytes in control spinal cords at 30 dpi are similar (Fig. 6). Quantification of the images reveal that β5i subunit labeling in EAE increases by 117 ± 34% ($p = 0.0059$) in neurons and by 94 ± 47% ($p = 0.0749$) in astrocytes, while levels of this subunit in oligodendrocytes are unchanged ($p = 0.3414$) (Fig. 7b). It is noteworthy that gray matter astrocytes have the same changes in proteasome composition in EAE as those present in the white matter (data not shown). Similarly, EAE oligodendrocytes do not display any changes in proteasome composition regardless whether they are in gray or white matter (data not shown). It is also interesting to mention that while β5 staining in control and EAE is exclusively cytoplasmic, β5i (particularly in EAE) was also present in the nucleus. This agrees with a previous observation that IFN-γ promotes the nuclear accumulation of immunoproteasomes in HeLa and Hep2 cells (Fabunmi *et al.*, 2000). In addition to neural cells, the immunoproteasome-specific β5i subunit is present in leukocytes located in the more peripheral regions of the spinal cord (Fig. S.1). In agreement with the western blot data, PA28 was barely expressed in control spinal cords. In EAE, PA28 expression was present in inflammatory cells (not shown) and astrocytes (Fig. S.2)

Increased expression of immunoproteasomes is likely due to activation of STAT-1 signaling pathway

It has been shown that IFN-γ augments the transcription of the immunoproteasome-specific subunits β1i, β2i and β5i (Aki *et al.*, 1994) via binding of STAT-1-dependent IRF-1 to IFN-γ regulatory elements in the promoter regions of these genes (Foss and Prydz, 1999). The expression of PA28 is also increased by IFN-γ (Groepttrup *et al.*, 1995). In addition, immunoproteasome subunits have NFκB response sequences within their promoters (Ferrington and Gregerson, 2012). As shown in Fig. 8a,b, the amount of phosphorylated STAT-1 (p-STAT-1) and IRF-1 in the nuclear fraction increases dramatically in the EAE spinal cord measured at 30 dpi, which clearly results from the ~18-fold rise in IFN-γ expression (Fig. 2c). In contrast, nuclear levels of NF-κB (p65 subunit) are unaltered in the disease (Fig. 8c). In sum, these data strongly suggest that expression of i-20S and PA28 particles in EAE is mainly the result of activation of the IFN-γ / STAT-1 / IRF-1 pathway.

Abnormal *Nfe2l1* (Nrf1) signaling may contribute to the reduced c-20S expression in EAE

Nrf1 is a transcription factor that upregulates the expression of all the proteasome subunit genes in a concerted manner, particularly during proteasome impairment (Radhakrishnan *et al.*, 2010; Lee *et al.*, 2013). There are several Nrf1 isoforms that derive from (1) alternative

splicing, (2) alternative initiation of translation, and (3) posttranslational processing (e.g. glycosylation, proteolysis) (Bugno *et al.*, 2015; Xiang *et al.*, 2018). We thought of the possibility that Nrf1 expression may be altered in EAE, which could result in decreased synthesis of constitutive proteasomes. To that end, we first measured *Nfe2l1* mRNA levels in the spinal cord during the course of EAE using a set of primers that recognizes all the transcripts. As shown in Fig. 9a, *Nfe2l1* gene expression in EAE declines starting at 9 dpi, with the difference being maximal between 14 and 21 dpi. It is noteworthy that the temporal pattern of mRNA expression of *Nfe2l1* is similar to that of *Psmb5* (Fig. 3). Western blot analysis of cytoplasmic fractions prepared from control and EAE spinal cords at 30 dpi, reveal the presence of six Nrf1-positive bands with molecular masses ranging from 25 kDa to 100 kDa (Fig. 9b). Of all these bands, only the 55 kDa band (Nrf1β) is present in the nucleus and its levels are reduced in EAE by 50.0 ± 10.0% (p= 0.0037) (Fig. 9c). When the films corresponding to the nuclear fractions are exposed for a longer time, the 100 kDa band (Nrf1α) becomes visible and its levels are also reduced in EAE (Fig. S.3). Double label-immunohistochemical analysis to identify the cells where Nrf1 is reduced were inconclusive due to the heterogeneous labeling of the nuclei in control (mostly diffuse) and EAE (mostly punctuate) spinal cords (data not shown).

Aside from stress-related stimuli, *Nfe2l1* expression is induced by growth factors through mTORC1-activation of the sterol regulatory element-binding protein 1 transcription factor (Zhang and Manning, 2015). However, we found that the levels of phospho-mTOR are significantly elevated in EAE measured at 30 dpi, implying that other factors may regulate Nrf1 transcription (Fig. 10a). One such molecule is the pre-B-cell leukemia homeobox-1 transcription factor (PBX1), which has been recently shown to directly induce Nrf1 gene expression (Villaescusa *et al.*, 2016). Interestingly, at 30 dpi, nuclear PBX1 levels are reduced in EAE spinal cords by 51.7 ± 3.7% (p= 0.0004) (Fig. 10b), suggesting that this phenomenon may underlie the *Nfe2l1* deficit in the disease.

Proteasome composition is also altered in the cerebella, but not the cerebra, of EAE mice.

Finally, we measured the expression of proteasomes and their activators in the cerebra and cerebella of EAE mice. Lesions in the cerebellum are different, both in location and intensity, than those in the spinal cord, while minimal pathological changes are known to occur in the cerebrum (Kuerten *et al.*, 2007). As shown in Fig. 11, the patterns of expression of the proteasome subunits β5, β5i and α, as well as the activator PA28α, in the EAE cerebellum are similar to those found in the spinal cord; specifically, there is an increase in the levels of i-20S and PA28 and a concomitant reduction in the amount of c-20S. However, the magnitude of the changes in the diseased cerebellum is smaller than those in the spinal cord. For instance, β5i, α1–3/5–7 and PA28α subunit levels in the cerebella of EAE mice rise by 53.6 ± 22%, 17.2 ± 4.4% and 271 ± 33%, respectively (Fig. 11), while amounts of these subunits in the EAE spinal cords increase by 1680 ± 585%, 75.7 ± 15.0% and 686 ± 158%, respectively (Fig. 4a). Similarly, β5 levels diminish by 25.2 ± 3.8% (p = 0.0211) in EAE cerebella versus 36.7 ± 7.8% in EAE spinal cords. In contrast to the findings in the spinal cord, the amount of the 19S subunit Rpt5 in the EAE cerebellum is unaltered. Analysis of EAE and control cerebra revealed no changes in the levels of any of these proteasome subunits except for a modest increase (68.7 ± 22.7%, p = 0.0174) in PA28α

levels. In sum, the magnitude of the changes in proteasome subunits in EAE are the highest in the spinal cord, followed by the cerebellum and the cerebrum. This correlates with the varying extents of inflammation and damage in these CNS areas. Interestingly, Nrf1β levels are also reduced in the cerebellum but not the cerebrum (Fig. S.4). Thus, while subunit displacement is likely to account for some of the decrease in the amounts of constitutive proteasomes in EAE, the contribution of Nrf1 deficiency to this phenomenon could also be significant.

Discussion

In this study, we describe the changes in the expression of proteasome particles and their activators in the spinal cords of EAE mice. The results clearly show that (1) there is a rise in i-20S and PA28 expression and a decline in c-20S expression in EAE, both at the mRNA and protein level; (2) among the three cell types studied, the changes are observed in neurons and astrocytes but not oligodendrocytes; (3) the increase in the amount of the i-20S-specific subunit β5i and PA28α/β in EAE correlates with the levels of IFN-γ, p-STAT-1 and IRF-1, but not with those of NFκB, suggesting that STAT-1 and/or IRF-1 dimers are responsible for induction of these subunits; (4) the decrease in the c-20S-specific β5 subunit mRNA and protein levels may also be due to reduced expression of Nrf1α and Nrf1β; and (5) impaired *Nfe2l1* mRNA expression is unlikely due to reduced mTOR signaling but could be the result of diminished PBX1 levels.

There is abundant biochemical and immunohistochemical data, including those presented in this study, showing that inflammation is a major feature of the EAE spinal cord. Local inflammation leads to the production of several pro-inflammatory cytokines, particularly IFN-γ, which are known to upregulate immunoproteasome subunits and the proteasome activator PA28 (Aki *et al.*, 1994; Groepttrup *et al.*, 1995). In line with this notion, we found that the amount of i-20S and PA28α/β, both mRNA and protein, is greatly elevated in EAE (Fig. 4). This is not surprising as the promoter regions of the inducible proteasome subunits and PA28 subunits contain binding sites for interferon consensus sequence-2 and gamma interferon activated sequence elements that bind STAT-1 and IRF-1 (Chatterjee-Kishore *et al.*, 2000), and the levels of both transcription factors are elevated in the nuclear fractions from EAE spinal cords (Fig. 8). The promoter of immunoproteasome and PA28 subunits also contain additional binding sites for other transcription factors, including three regions of consensus sequence for NF-κB binding (Ferrington and Gregerson, 2012). Interestingly, nuclear NF-κB levels were unchanged in EAE, suggesting that IFN-γ is regulating immunoproteasome expression mostly via STAT-1 and IRF-1. The lack of increased NF-κB signaling in EAE was surprising since the nuclear levels of this transcription factor are known to be up-regulated by pro-inflammatory cytokines like TNF-α (Hayden and Ghosh, 2014) and IL-1β (McDonald *et al.*, 1997) as well as by oxidative stress (Morgan and Liu, 2011), all of which are elevated in EAE (Fig. 2d–f). Perhaps NF-κB is elevated in a small subset of cells like microglia or lymphocytes, and therefore such an increase is not detected when one analyzes total spinal cord proteins.

Concomitant with the rise in the concentration of i-20S and 11S particles in EAE, we discovered a reduction in the amount of c-20S, suggesting the displacement of housekeeping

proteasome subunits by immuno-subunits. In support of this idea, we observed that neural cells in EAE spinal cords where β5i expression is increased (i.e. neurons and astrocytes) have low β5 expression. Similarly, EAE oligodendrocytes show no changes in either β5i or β5 expression. Moreover, in the EAE cerebellum, where the increase in the amount of β5i is less pronounced than that in the spinal cord, the reduction in β5 levels is smaller. Proteasome subunit displacement is a well-characterized post-translational process achieved by competition of the inducible subunits with the respective constitutive subunits for a common assembly site within the 20S particle (Früh *et al.*, 1994). The preferential incorporation of all three immuno-subunits (β1i, β2i and β5i) is assisted by the proteasome maturation protein (POMP). This protein binds the pro-peptide of β5i with greater affinity than that of β5, resulting in preferred formation of i-20S over c-20S particles (Heink *et al.*, 2005). Interestingly, POMP expression is upregulated by IFN-γ (Burri *et al.*, 2000), whose levels are augmented in EAE (Fig 2c). Furthermore, p-mTOR (Yun *et al.*, 2016), which is also elevated in EAE (Fig. 10a), promotes the formation of immunoproteasomes by making the immuno-subunits available to POMP via PRAS40 activation. Thus, the conditions present in the EAE spinal cord enable the preferential formation of i-20S over c-20S core particles.

It is important to note that immune cells and microglia may contribute to the western blot and qPCR values determined in spinal cord homogenates. Indeed, we found that $CD45^+$ cells contain significant amounts of β5i (Fig. S.1). Also, we have previously shown that $CD3^+$ cells and microglia in EAE cerebellum express β5i (Zheng et al., 2012). However, even if microglia and immune cells were to express only immunoproteasomes, that would not explain the decrease in the levels of constitutive particles in EAE from 4.67 to 2.98 pmol/mg protein. Thus, the data in the homogenates cannot be explained simply by the contribution of these non-neural cells. Most importantly, the presence of immunoproteasomes in other CNS cells does not change the fact that c-20S is being replaced with i-20S in EAE neurons and astrocytes, as demonstrated by immunohistochemical analysis.

While subunit displacement is likely one important reason for the reduced levels of constitutive proteasomes in EAE, it does not explain why *Psmb5* mRNA levels are also diminished in the disease (Figs. 3 and 4). STAT-3 has been shown to increase *Psmb5* mRNA and protein levels, and the amount of constitutive proteasome (Vangala *et al.*, 2014). However, phospho-STAT-3 levels are augmented in EAE spinal cords (Hou *et al.*, 2017), suggesting that reduction of *Psmb5* mRNA expression cannot not be attributed to impaired STAT-3 signaling. The promoter regions of all the constitutive proteasome subunits and those that make up the 11S and 19S complexes have EpRE that can bind to and became activated by Nrf1 and Nrf2 (Pickering *et al.*, 2012). However, while both transcription factors can increase proteasome subunit expression, only Nrf1 is required for upregulation of proteasome genes in response to proteasome inhibition (Radhakrishnan *et al.*, 2010). Furthermore, late-stage deletion of Nrf1 in neuronal cells leads to impaired proteasome function due to down-regulation of proteasomal genes that encode the catalytic subunits (Lee *et al.*, 2011). These studies point to the critical role of Nrf1 in the biogenesis of constitutive proteasomes and prompted us to explore the possibility that expression of this transcription factor is diminished in EAE. In the present study, we discovered that *Nfe2l1*

mRNA levels, utilizing a set of primers that measure all transcripts, are reduced in EAE spinal cords with a temporal pattern similar to that of *Psmb5* mRNA. The reason for diminished Nfe2l1 mRNA expression in EAE is unknown but it does not appear to be the result of reduced mTOR signaling (Fig. 10a). Interestingly, we found a decline in PBX1 content in EAE spinal cords, which could underlie the reduced Nrf1 expression (Fig. 10b). PBX1 has been recently shown to activate *Nfe2l1* expression to promote neuronal survival (Villaescusa *et al.*, 2016). Furthermore, those studies also revealed that both PBX1 and Nrf1 are absent in *substantia nigra* neurons from Parkinson's disease patients, suggesting an impaired PBX1-Nrf1 pathway in neurodegeneration.

The *Nfe2l1* gene can yield multiple mRNA transcripts that can undergo alternative initiation of translation generating distinct polypeptide isoforms. These forms can also be modified by glycosylation and proteolytic cleavage, rendering several bands on SDS-gels with molecular masses ranging from 25 kDa to 140 kDa (Bugno *et al.*, 2015; Xiang *et al.*, 2018). The four major forms are the full-length Nrf1 (Nrf1α, ~100 kDa on SDS-gradient gels), Nrf1β (~55 kDa), generated through in-frame translation, Nrf1γ (~36 kDa), produced by a separate in-frame translation starting codon, and Nrf1δ (~ 25 kDa) that seems to arise from proteolytic cleavage of Nrf1γ (Zhang *et al.*, 2014; Bugno *et al.*, 2015;). Nrf1α exhibits a stronger transactivation activity than Nrf1β (Caterina *et al.*, 1994; Prieschl *et al.*, 1998; Zhang *et al.*, 2014), while Nrf1γ/ δ are dominant-negative forms that interfere with the functional association of Nrf1α or Nrf2 to small musculoaponeurotic fibrosarcoma proteins and down-regulate the expression of EpRE-containing genes (Zhang *et al.*, 2014). Our present work reveals that Nrf1β is the major Nrf1 species present in the nuclear fraction along with a small amount of Nrf1α, and that the levels of both of these positive activators of proteasome expression decline in EAE. A number of additional Nrf1-positive bands were detected on western blots of the cytosolic fraction; these include the 85 kDa and 76 kDa species, which are considered proteolytic fragments of Nrf1α, a 46 kDa form (Nrf1β2) that derives from Nrf1β cleavage, and a 25 kDa form that is likely to be Nrf1δ. However, none of these species are present in the nuclear fractions from the spinal cords and thus were not quantified. It is important to note that most studies in the literature assign functionality to Nrf1 isoforms based on their levels in cell homogenates without determining whether or not they are present in the nucleus.

In summary, we have obtained evidence that two important mechanisms, subunit displacement and impaired *Nfe2l1* signaling, may be the cause for the reduced amounts of constitutive proteasomes in neurons and astrocytes during inflammatory demyelination. Because constitutive proteasomes and immunoproteasomes are equally effective at removing ubiquitinated (Nathan *et al.*, 2013) and oxidized proteins (Pickering *et al.*, 2010; Zheng *et al.*, 2012), it is fair to conclude that the overall capacity of these cells to eliminate damaged proteins is augmented in EAE and helps prevent the toxic protein accumulation at the peak of the disease. In a previous study on proteasome composition in the EAE cerebellum, we discovered that as the disease progresses from the inflammatory to the neurodegenerative phase, immunoproteasome levels return to normal without being counterbalanced by a rise in the amounts of constitutive proteasomes (Zheng *et al.*, 2012). This suggests that impaired synthesis of constitutive proteasomes in chronic EAE, caused perhaps by deficient Nrf1 signaling, could be an important pathophysiological mechanism.

Involves human subjects:
If yes: Informed consent & ethics approval achieved:
=> if yes, please ensure that the info “Informed consent was achieved for all subjects, and the experiments were approved by the local ethics committee.” is included in the Methods.

ARRIVE guidelines have been followed:
Yes
=> if it is a Review or Editorial, skip complete sentence => if No, include a statement: “ARRIVE guidelines were not followed for the following reason: “
(edit phrasing to form a complete sentence as necessary).
=> if Yes, insert “All experiments were conducted in compliance with the ARRIVE guidelines.” unless it is a Review or Editorial

Supplementary Material

Refer to Web version on PubMed Central for supplementary material.

Acknowledgements

This work was supported by PHHS grants NS082805 from the National Institutes of Health.

Abbreviations:

α7 (*Psma7*)	20S subunit α7
β5 (*Psmb5*)	c-20S subunit β5
β5i (*Psmb8*)	i-20S inducible subunit β5
CFA	complete Freund’s adjuvant
c-20S	constitutive-20S particle
EAE	experimental autoimmune encephalomyelitis
GAPDH	glyceraldehyde 3-phosphate dehydrogenase
H3	histone H3
i-20S	immuno-20S particle
IL-1β	interleukin-1β
IFN-γ	interferon-γ
IRF-1	interferon regulatory factor-1

MOG	myelin oligodendrocyte glycoprotein
mTOR	mammalian target of rapamycin
Nrf1 (*Nfe2l1*)	nuclear factor (erythroid-derived 2)-like 1
NF-κB	nuclear factor kappa-light-chain-enhancer of activated B cells
PA28	11S regulatory particle
PA28α (*Psme1*)	PA28 subunit α
PA28β (*Psme2*)	PA28 subunit β
PA700	19S regulatory particle
PBX1	pre-B-cell leukemia homeobox-1 transcription factor
qPCR	quantitative polymerase chain reaction
POMP	proteasome maturation protein
Rpt5 (*Psmc3*)	19S regulatory subunit 6A
RRID	research resource identifier
STAT-1	signal transducer and activator of transcription 1
TNF-α	tumor necrosis factor-α

References

Aki M, Shimbara N, Takashina M, Akiyama K, Kagawa S, Tamura T, Tanahashi N, Yoshimura T, Tanaka K and Ichihara A (1994) Interferon-gamma induces different subunit organizations and functional diversity of proteasomes. J. Biochem 115, 257–269. [PubMed: 8206875]

Biswas M and Chan JY (2010) Role of Nrf1 in antioxidant response element-mediated gene expression and beyond. Toxicol. Appl. Pharmacol 244, 16–20. [PubMed: 19665035]

Bugno M, Daniel M, Chepelev NL and Willmore WG (2015) Changing gears in Nrf1 research, from mechanisms of refulation to its role in disease and prevention. Biochim. Biophys. Acta 1849, 1260–1276. [PubMed: 26254094]

Burri L, Hockendorff J, Boehm U, Klamp T, Dohmen RJ and Levy F (2000) Identification and characterization of a mammalian protein interacting with 20S proteasome precursors. Proc. Natl. Acad. Sci. USA 97, 10348–10353. [PubMed: 10973495]

Braun B, Glickman M, Kraft R, Dahlmann B, Kloetzel PM, Finley D and Schmidt M (1999) The base of the proteasome regulatory particle exhibits chaperone-like activity. Nat. Cell Biol 1, 221–226. [PubMed: 10559920]

Caterina JJ, Donze D, Sun CW, Ciavatta DJ and Townes TM (1994) Cloning and functional characterization of Lcr-F1 - a bzip transcription factor that activates erythroid-specific, human globin gene - expression. Nucleic Acids Res. 22, 2383–2391. [PubMed: 8036168]

Chatterjee-Kishore M, Wright KL, Ting GP and Stark GR. (2000) How Stat1 mediates constitutive gene expression: a complex of unphosphorylated Stat1 and IRF1 supports transcription of the LMP2 gene. EMBO J. 19: 4111–4122. [PubMed: 10921891]

Coux O, Tanaka K and Goldberg AL (1996) Structure and functions of the 20S and 26S proteasomes. Annu. Rev. Biochem 65, 801–847. [PubMed: 8811196]

Ethen CM, Hussong SA, Reilly C, Feng X, Olsen TW and Ferrington DA (2007) Transformation of the proteasome with age-related macular degeneration. FEBS Lett. 581, 885–890. [PubMed: 17289037]

Fabunmi RP, Wigley WC, Thomas PJ and DeMartino GN (2000) Interferon-γ regulates accumulation of the proteasome PA28 and immunoproteasomes at nuclear PML bodies. J. Cell Sci 114, 29–36.

Ferrington DA and Gregerson DS (2012). Immunoproteasomes: structure, function, and antigen presentation. Prog. Mol. Biol. Transl. Sci 109, 75–112. [PubMed: 22727420]

Foss GS and Prydz H (1999) Interferon regulatory factor-1 mediates the interferon-c induction of the human immunoproteasome subunit multicatalytic endopeptidase complex-like-1. J. Biol. Chem 274, 35196–35202. [PubMed: 10575004]

Früh K, Gossen M, Wang K, Bujard H, Peterson P and Yang Y (1994) Displacement of housekeeping proteasome subunits by MHC-encoded LMPs: a newly discovered mechanism for modulating the multicatalytic proteinase complex. EMBO J. 13, 3236–3244. [PubMed: 8045254]

Gold R, Hartung HP and Toyka KV (2000) Animal models for autoimmune demyelinating disorders of the nervous system. Mol. Med. Today 6, 88–91. [PubMed: 10652482]

Groettrup M, Ruppert T, Kuehn L, Seeger M, Standera S, Koszinowski U and Kloetzel PM (1995) The interferon-γ-inducible 11S regulator (PA28) and the LMP2/LMP7 subunits govern the peptide production by the 20S proteasome in vitro. J. Biol. Chem 270, 23808–23815. [PubMed: 7559557]

Hayden MS and Ghosh S (2014) Regulation of NF-κB by TNF family cytokines. Semin. Immunol 26, 253–266. [PubMed: 24958609]

Hou H, Miao J, Cao R, Han M, Sun Y, Liu X and Guo L (2014) Rapamycin ameliorates experimental autoimmune encephalomyelitis by suppressing the mTOR-STAT3 pathway. Neurochem. Res 42, 2831–2840.

Heink S, Ludwig D, Kloetzel PM and Kruger E (2005) IFN-gamma-induced immune adaptation of the proteasome system is an accelerated and transient response. Proc. Natl. Acad. Sci. USA 102: 9241–9246. [PubMed: 15944226]

Hu CL, Nydes M, Shanley KL, Morales-Pantoja IE, Howard TA and Bizzozero OA (2019) Reduced expression of the ferroptosis inhibitor glutathione peroxidase-4 in multiple sclerosis and experimental autoimmune encephalomyelitis. J. Neurochem 148, 426–439. [PubMed: 30289974]

Hussong SA, Kapphahn RJ, Phillips SL, Maldonado M and Ferrington DA (2010) Immunoproteasome deficiency alters retinal proteasome's response to stress.J. Neurochem 113, 1481–1490. [PubMed: 20345760]

Kobayashi A, Kang MI, Okawa H, Ohtsuji M, Zenke Y, Chiba T, Igarashi K and Yamamoto M (2004) Oxidative stress sensor Keap1 functions as an adaptor for Cul3-based E3 ligase to regulate proteasomal degradation of Nrf2. Mol. Cell. Biol 24, 7130–7139. [PubMed: 15282312]

Kuerten S, Kostova-Bales DA, Frenzel LP, Tigno JT, Tary-Lehmann M, Angelov DN and Lehmann PV (2007) MP4- and MOG:35–55-induced EAE in C57BL/6 mice differentially targets brain, spinal cord and cerebellum. J. Neuroimmunol 189, 31–40. [PubMed: 17655940]

Lee CS, Lee C, Hu T, Nguyen JM, Zhang J, Martin MV, Vawter MP, Huang EJ and Chan JY (2011) Loss of nuclear factor E2-related factor 1 in the brain leads to dysregulation of proteasome gene expression and neurodegeneration. Proc. Natl. Acad. Sci. USA 108, 8408–8413. [PubMed: 21536885]

Lee CS, Ho DV and Chan JY (2013) Nuclear factor-erythroid 2-related factor 1 regulates expression of proteasome genes in hepatocytes and protects against endoplasmic reticulum stress and steatosis in mice. FEBS J. 280, 3609–3620. [PubMed: 23702335]

Livak KJ and Schmittgen TD (2001) Analysis of relative gene expression data using real-time quantitative PCR and the 2(-Delta Delta C(T)) method. Methods 25, 402–408. [PubMed: 11846609]

McDonald PP Bald A and Cassatella MA (1997) Activation of NF-κB pathway by inflammatory stimuli in human neutrophils. Blood 89, 3421–3433. [PubMed: 9129050]

Morales Pantoja I, Hu C, Perrone-Bizzozero NI, Zheng J and Bizzozero OA (2016) Nrf2-dysregulation correlates with reduced synthesis and low glutathione levels in experimental autoimmune encephalomyelitis. J. Neurochem 139: 640–650. [PubMed: 27579494]

Morgan MJ and Liu Z (2011) Crosstalk of reactive oxygen species and NF-κB signaling. Cell Res. 21, 103–115. [PubMed: 21187859]

Motohashi H, Katsuoka F, Shavit JA, Engel JD and Yamamoto M (2000) Positive or negative MARE-dependent transcriptional regulation is determined by the abundance of small Maf proteins. Cell 103, 865–875. [PubMed: 11136972]

Nathan JA, Spinnenhim V, Schmidtke G, Basler M, Goettrup M and Goldberg AL (2013) Immuno- and constitutive proteasomes do not differ in their abilities to degrade ubiquitinated proteins. Cell 152, 1184–1194. [PubMed: 23452861]

Pickering AM, Koop AL, Teoh CY, Ermak G, Grune T, Davies KJA (2010) The immunoproteasome, the 20S proteasome and the PA28αβ proteasome regulator are oxidative stress adaptive proteolytic complexes. Biochem J. 432, 585–594. [PubMed: 20919990]

Pickering AM, Linder RA, Zhang H, Forman HJ and Davies KJA (2012) Nrf2-dependent induction of proteasome and PA28ab regulator are required for adaptation to oxidative stress. J. Biol. Chem 287, 10021–10031. [PubMed: 22308036]

Prieschl EE, Novotny V, Csonga R, Jaksche D, Elbe-Bürger A, Thum W, Auer MA, Stingl G and Baumruker T (1998) A novel splice variant of the transcription factor Nrf1 interacts with the TNFα promoter and stimulates transcription. Nucleic Acids Res. 26, 2291–2297. [PubMed: 9580677]

Radhakrishnan SK, Lee CS, Young P, Beskow A, Chan JY and Deshaies RJ (2010) Transcription factor Nrf1 mediates the proteasome recovery pathway after proteasome inhibition in mammalian cells. Mol. Cell 38, 17–28. [PubMed: 20385086]

Rechsteiner M and Hill CP (2005) Mobilizing the proteolytic machine: cell biological roles of proteasome activators and inhibitors. Trends Cell. Biol 15, 27–33. [PubMed: 15653075]

Rivett AJ and Hearn AR (2004) Proteasome function in antigen presentation: immunoproteasome complexes, peptide production and interactions with viral proteins. Curr. Protein Pept. Sci 5, 153–161. [PubMed: 15180520]

Seifert U, Lukasz P, Ebstein F, Bech-Otschir D, Voigt A, Schröter F, Prozorovski T, Lange N, Steffen J, Rieger M, Kuckelkorn U, Aktas O, Kloetzel P and Krüger E (2010) Immunoproteasomes preserve protein homeostasis upon interferon-induced oxidative stress. Cell 142, 613–624. [PubMed: 20723761]

Vandesompele J, DePreter K, Pattyn F, Poppe B, Van Roy N, DePaepe A and Speleman F (2002) Accurate normalization of real-time quantitative RT-PCR data by geometric averaging of multiple internal control genes. Genome Biology 3, 1–11.

Vangala JR Dudem S, Jain N and Kalivendi SV (2014) Regulation of PSMB5 protein and β subunits of mammalian proteasome by constitutively activated signal transducer and activator of transcription 3 (STAT3). J. Biol. Chem 289, 12612–12622. [PubMed: 24627483]

Venugopal R and Jaiswal AK (1998) Nrf2 and Nrf1 in association with Jun proteins regulate antioxidant response element-mediated expression and coordinated induction of genes encoding detoxifying enzymes. Oncogene 17, 3145–3256. [PubMed: 9872330]

Villaescusa JC, Li B, Toledo EM, Riveti P, Yang S, Scott SRW, Kaiser K, Islam S, Gyllborg D, Laguna-Goya R, Landreh M, Lönnerberg P, Falk A, Bergman T, Barker RA, Linnarsson S, Selleri L and Arenas E (2016) A PBX1 transcriptional network controls dopaminergic neuron development and is impaired in Parkinson's disease. EMBO J. 35, 1963–1978. [PubMed: 27354364]

Xiang Y, Wang M, Hu S, Qiu L, Yang F, Xhang Z, Yu S, Pi J and Zhang Y (2018) Molecular mechanisms controlling the multistage post-translational processing of endogenous Nrf1a/TCF11 proteins to yield distinct isoforms within the coupled positive and negative feedback circuits. Toxicol. Appl. Pharm, 360: 212–235.

Yun YS, Kim KH, Tschida B, Sachs Z, Noble-Orcutt KE, Moriarity BS, Ai T, Ding R, Williams J, Chen L, Largaespada D and Kim DH (2016) mTORC1 coordinated protein synthesis and immunoproteasome formation via PRAS40 to prevent accumulation of protein stress. Mol. Cell 61, 625–639. [PubMed: 26876939]

Zhang Y and Manning BD (2015) mTORC1 signaling activates NRF1 to increase cellular proteasome levels. Cell Cycle 14, 2011–2017. [PubMed: 26017155]

Zhang Y, Qiu L, Li S, Xiang Y, Chen J and Ren Y (2014) The C-terminal domain of Nrf1 negatively regulates the full-length CNC-bZIP factor and its shorter isoform LCRF1/Nrf1β; both are also inhibited by the small dominant-negative Nrf1γ/δ isoforms that down-regulate ARE-battery gene expression. PLoS One 9, e109159 [PubMed: 25290918]

Zheng J and Bizzozero OA (2010) Reduced proteasomal activity contributes to the accumulation of carbonylated proteins in chronic experimental autoimmune encephalomyelitis. J. Neurochem 115, 1556–1567. [PubMed: 20950414]

Zheng J and Bizzozero OA (2011) Decreased activity of the 20S proteasome in the brain white matter and gray matter of patients with multiple sclerosis. J. Neurochem 117, 143–153. [PubMed: 21235577]

Zheng J, Dasgupta A and Bizzozero OA (2012) Changes in 20S subunit composition are largely responsible for altered proteasomal activities in experimental autoimmune encephalomyelitis. J. Neurochem 121: 486–494. [PubMed: 22353035]

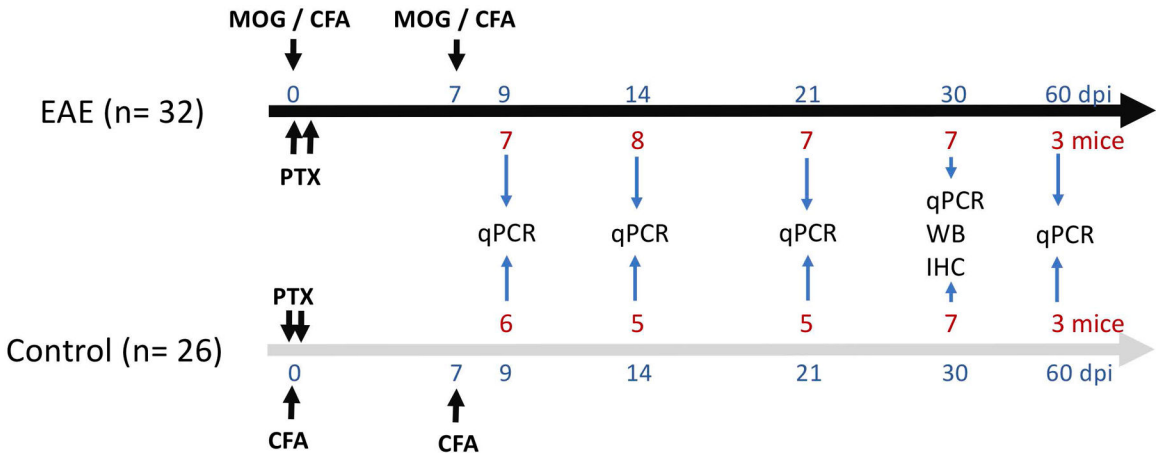

Fig. 1 –.

Schematic diagram showing the timeline of the EAE study design / procedures. WB, western blot; IHC, immunohistochemistry.

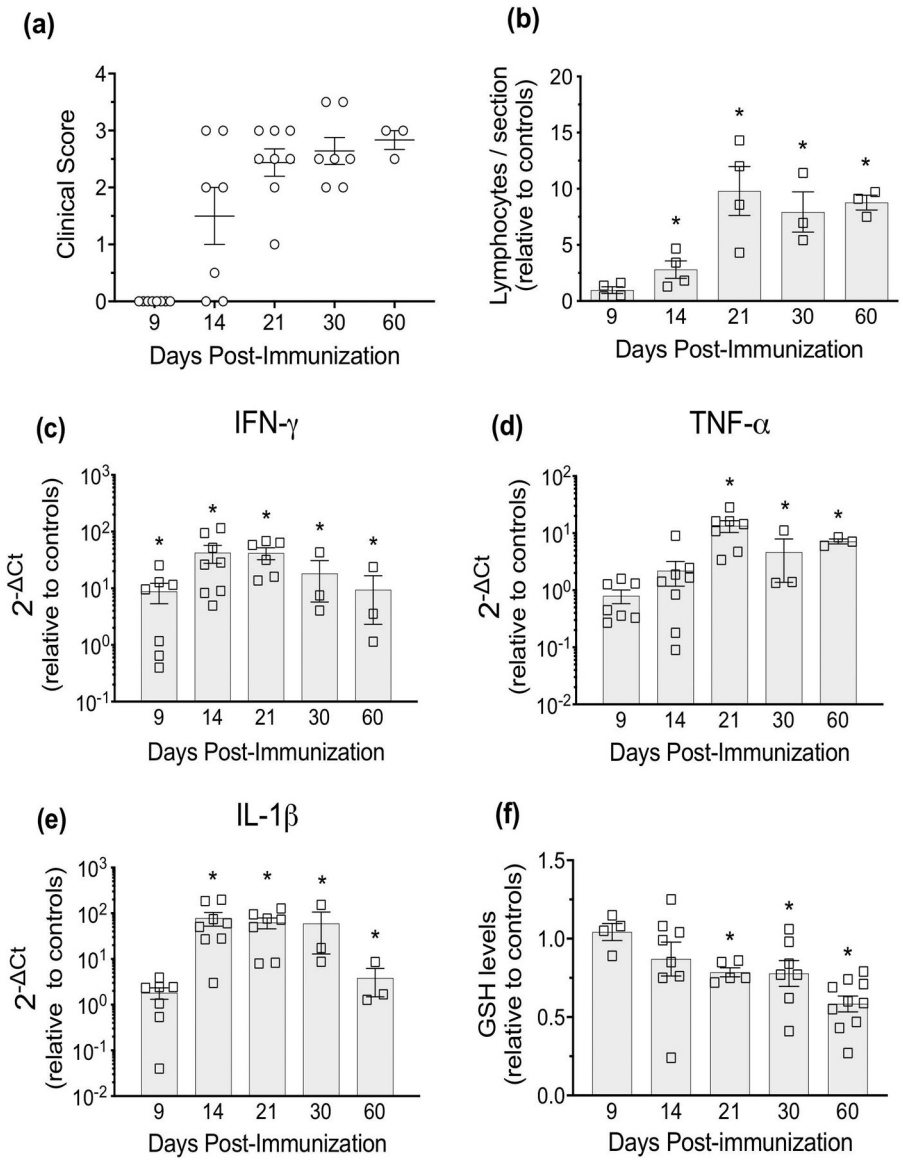

Fig. 2 –.

Elevated inflammation and oxidative stress during the course of EAE. EAE was induced in C57BL/6 female mice by active immunization with $MOG_{35–55}$ peptide in CFA. **(a)** Animals were monitored daily for signs of clinical disease, and symptoms were scored as indicated in the text. Dots represent the final clinical score of each of the 32 EAE mice used in the study. Control animals did not exhibit neurological symptoms (i.e. score = 0). **(b)** The number of lymphocytes per spinal cord section were assessed by hematoxylin and eosin staining. **(c-e)** IFN-γ, TNF-α and IL-1β mRNA levels during the course of the disease were determined by qPCR. **(f)** Total GSH levels were measured using the enzymatic recycling assay and data shown was taken from one of our previous publications (Morales Pantoja *et al.*, 2016). Each point represents one animal. Values are expressed relative to controls. Bars and horizontal lines show the mean ± SEM of 3–8 animals. Asterisks denote values that are statistically different ($p<0.05$) from their respective controls.

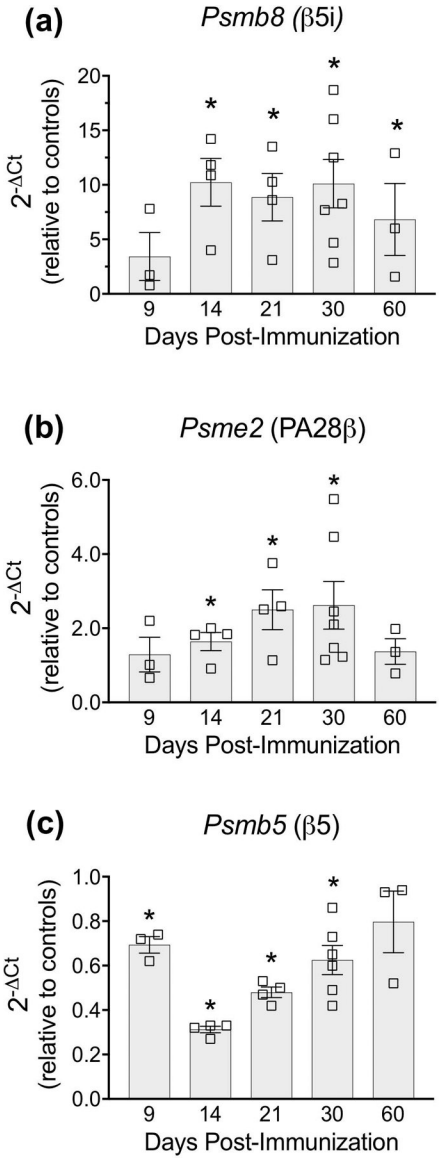

Fig. 3 –.

Altered gene expression of proteasomes, immunoproteasomes and PA28 during the course of EAE (9 – 60 dpi). **(a)** Proteasome subunit β5i (*Psmb8*), **(b)** PA28β (*Psme2*) and **(c)** proteasome subunit β5 (*Psmb5*) mRNA levels in the spinal cords of control and EAE mice were determined by qPCR. Each point represents one animal. Values are expressed relative to controls. Bars and horizontal lines show the mean ± SEM of 3–7 animals. Asterisks denote values that are statistically different ($p<0.05$) from their respective controls.

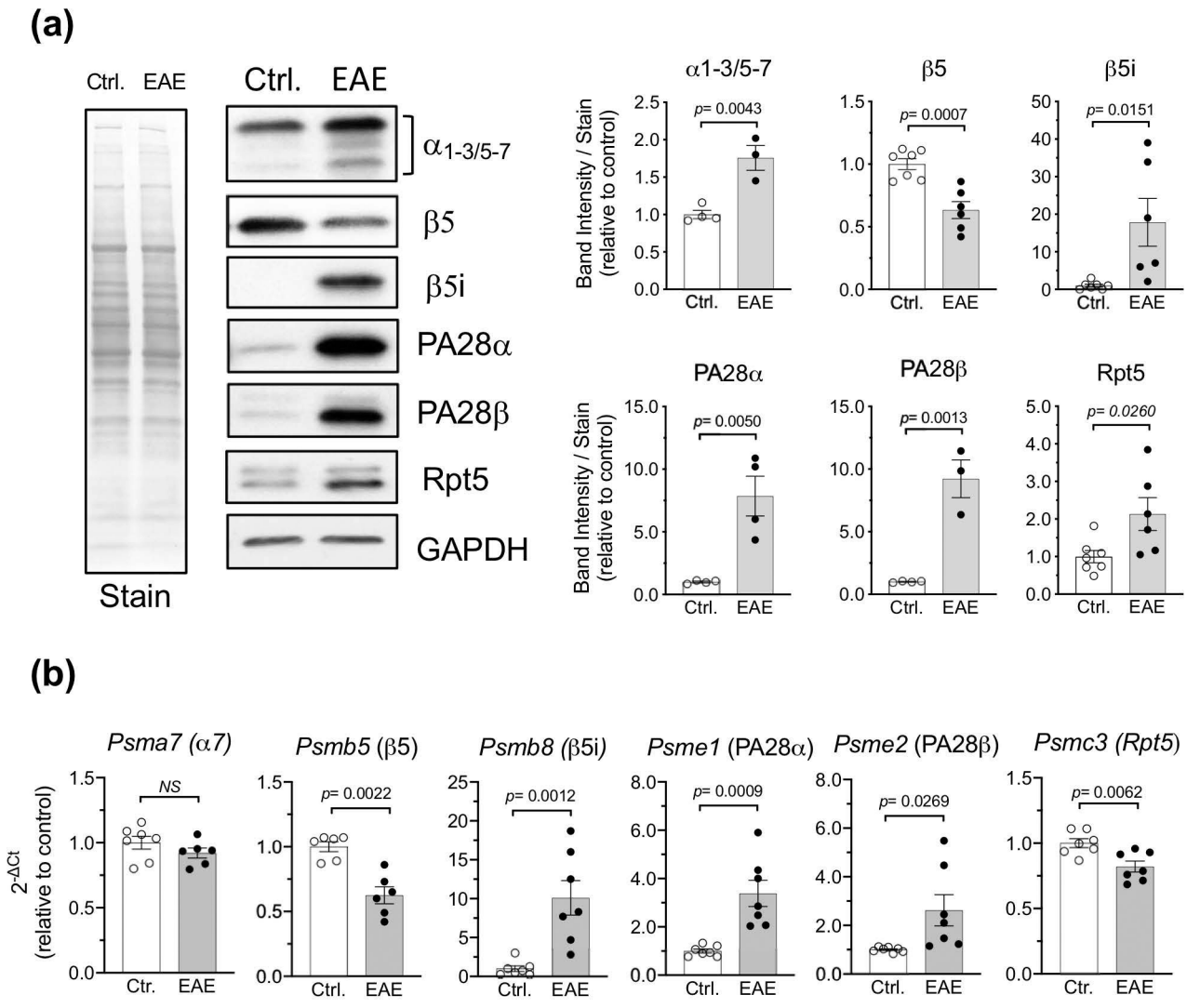

Fig. 4 –.

Reduced expression of constitutive proteasomes and increased expression of immunoproteasomes and the 11S activator in the EAE spinal cord**. (a)** Levels of subunits α1–3/5–7, β5, β5i, PA28α, PA28β and Rpt5 in control and EAE spinal cords at 30 dpi were determined by western blot analysis. Left panel shows representative western blots of the analyzed subunits. **(b)** *Psma7* (α7), *Psmb5* (β5), *Psmb8* (β5i), *Psme1* (PA28α), *Psme2* (PA28β) and *Psmc3* (Rpt5) mRNA levels in the spinal cords of control and EAE mice at 30 dpi were determined by qPCR. In both panels, each point represents one animal. Values are expressed relative to controls. Bars and horizontal lines depict the mean ± SEM of 3–7 animals. Statistical significance was determined by Student's *t*-test. *NS*, not significant.

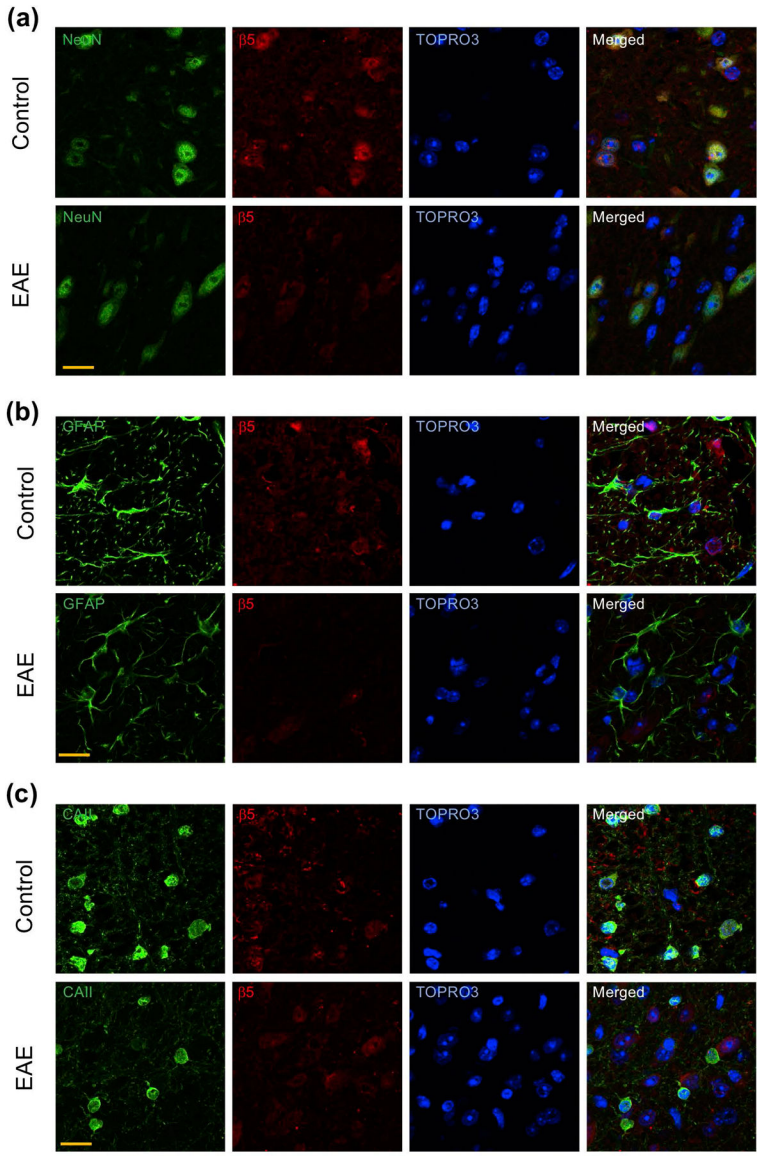

Fig. 5 –.

Representative double-label immunofluorescence images of lumbar spinal cord sections of control and EAE mice at 30 dpi depicting the expression of the c-20S-specific subunit β5 in neurons **(a)**, astrocytes **(b)** and oligodendrocytes **(c)**. Spinal cord sections (5 μm-thick) from control and EAE mice were co-stained with anti-β5 antibody and either anti-NeuN (neurons), anti-GFAP (astrocytes) or anti-CAII (mature oligodendrocytes) antibody, and images were visualized by confocal microscopy. Red channel is for β5 while green channel is for various cell markers. Nuclei were labeled with TO-PRO-3. Bars at lower left of each panel represent 20 μm in length.

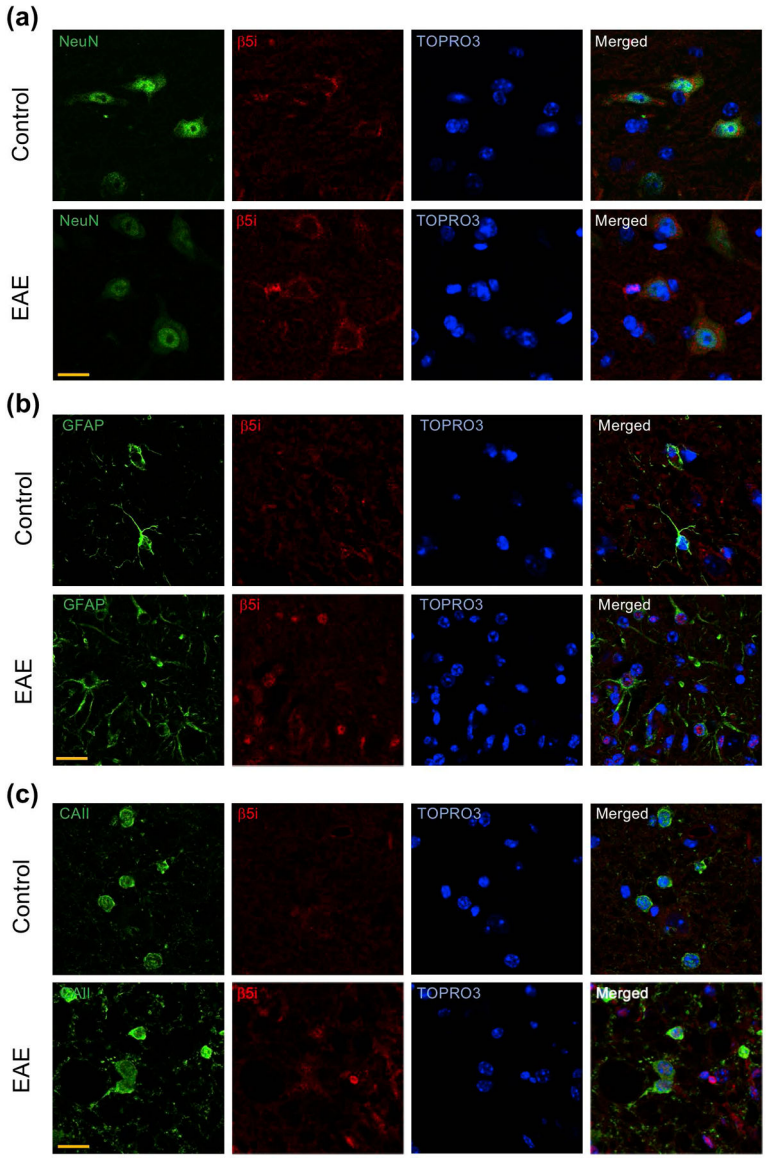

Fig. 6 –.

Representative double-label immunofluorescence images of lumbar spinal cord sections of control and EAE mice at 30 dpi depicting the expression of the i-20S-specific subunit β5i in neurons **(a)**, astrocytes **(b)** and oligodendrocytes **(c)**. Spinal cord sections (5 μm-thick) from control and EAE mice were co-stained with anti-β5i antibody and either anti-NeuN (neurons), anti-GFAP (astrocytes) or anti-CAII (mature oligodendrocytes) antibody, and images were visualized by confocal microscopy. Red channel is for β5i while green channel is for various cell markers. Nuclei were labeled with TO-PRO-3. Bars at lower left of each panel represent 20 μm in length.

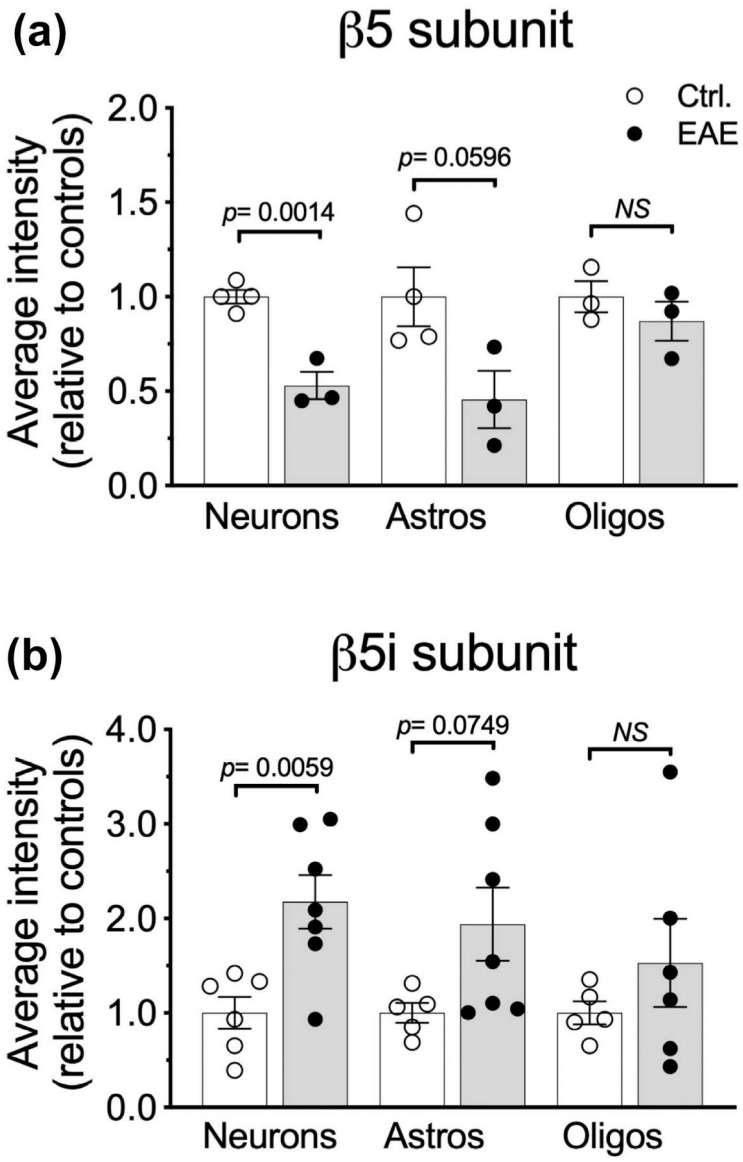

Fig. 7 –.

Differential expression of proteasome subunits β5 **(a)** and β5i **(b)** in neurons, astrocytes (astros) and oligodendrocytes (oligos) in EAE spinal cords at 30 dpi. Double immunofluorescence confocal analysis to estimate the average β5 and β5i fluorescence intensity in neurons, astrocytes and oligodendrocytes was performed as described in "Materials and Methods". Each point represents one animal. Values are expressed relative to controls. Bars and horizontal lines depict the mean ± SEM of 3–7 animals. Statistical significance was determined by Student's *t*-test. *NS*, not significant.

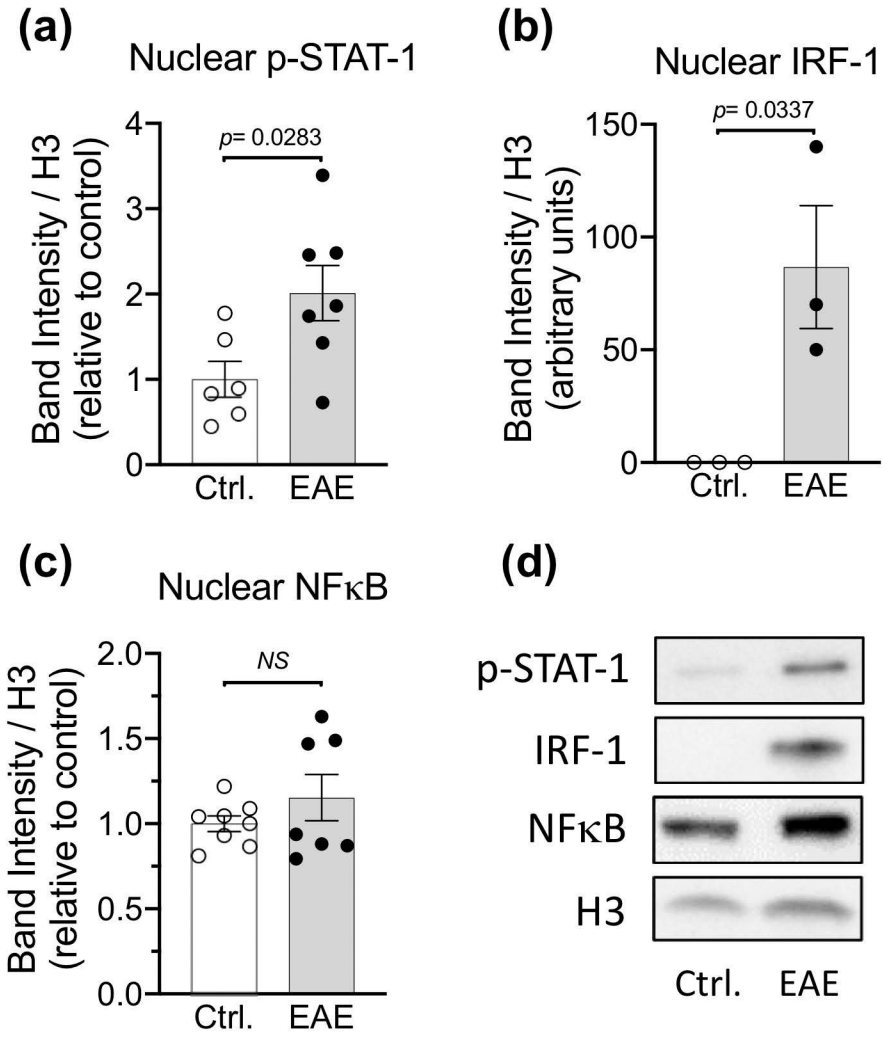

Fig. 8 –.

Augmented nuclear levels of p-STAT-1 and IRF-1, but not NFκB, in the EAE spinal cord. Levels of p-STAT-1 **(a)**, IRF-1 **(b)** and NFκB **(c)** in the nuclear fractions from control and EAE spinal cords at 30 dpi were determined by western blot analysis. Band intensities were corrected by the amount of histone H3 in the same gel lanes. Each point represents one animal. Values are expressed relative to controls except for panel b, where IRF-1 was undetectable in the control mice. Bars and horizontal lines depict the mean ± SEM of 3–7 animals. Statistical significance was determined by Student's *t*-test. *NS*, not significant. **(d)** Representative western blots of the analyzed proteins.

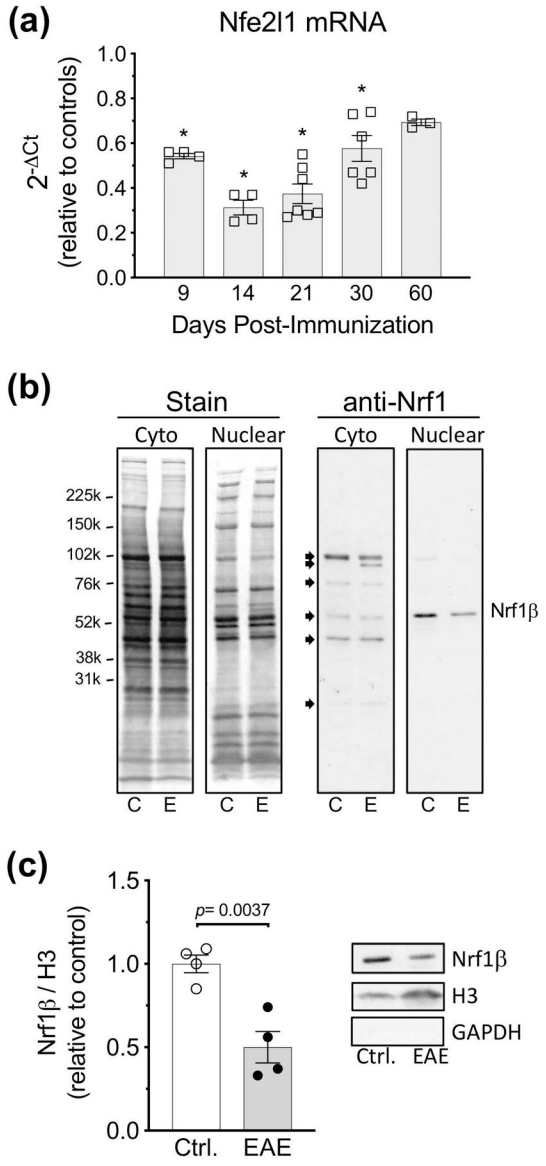

Fig. 9 –.

Decreased Nrf1 mRNA and protein expression in the EAE spinal cord. **(a)** *Nfe2l1* mRNA levels in the spinal cords of control and EAE mice were determined by qPCR. Each point represents one animal. Values are expressed relative to controls. Bars and horizontal lines show the mean ± SEM of 3–7 animals. Asterisks denote values that are statistically different ($p<0.05$) from their respective controls. **(b)** Cytoplasmic and nuclear proteins from control and EAE spinal cords at 30 dpi were analyzed by western blot using an antibody against Nrf1. The cytoplasmic fraction shows six Nrf1-positive bands with molecular masses ranging from 25 kDa to 100 kDa (arrows) but only the 55 kDa band (Nrf1β) is present in the nuclear fraction. **(c)** Band intensities corresponding to Nrf1β in the nuclear fraction were corrected by the amount of histone H3 in the same gel lanes. Each point represents one animal. Values are expressed relative to controls. Bars and horizontal lines depict the mean ±

SEM of 4 animals per experimental group. Statistical significance was determined by Student's *t*-test.

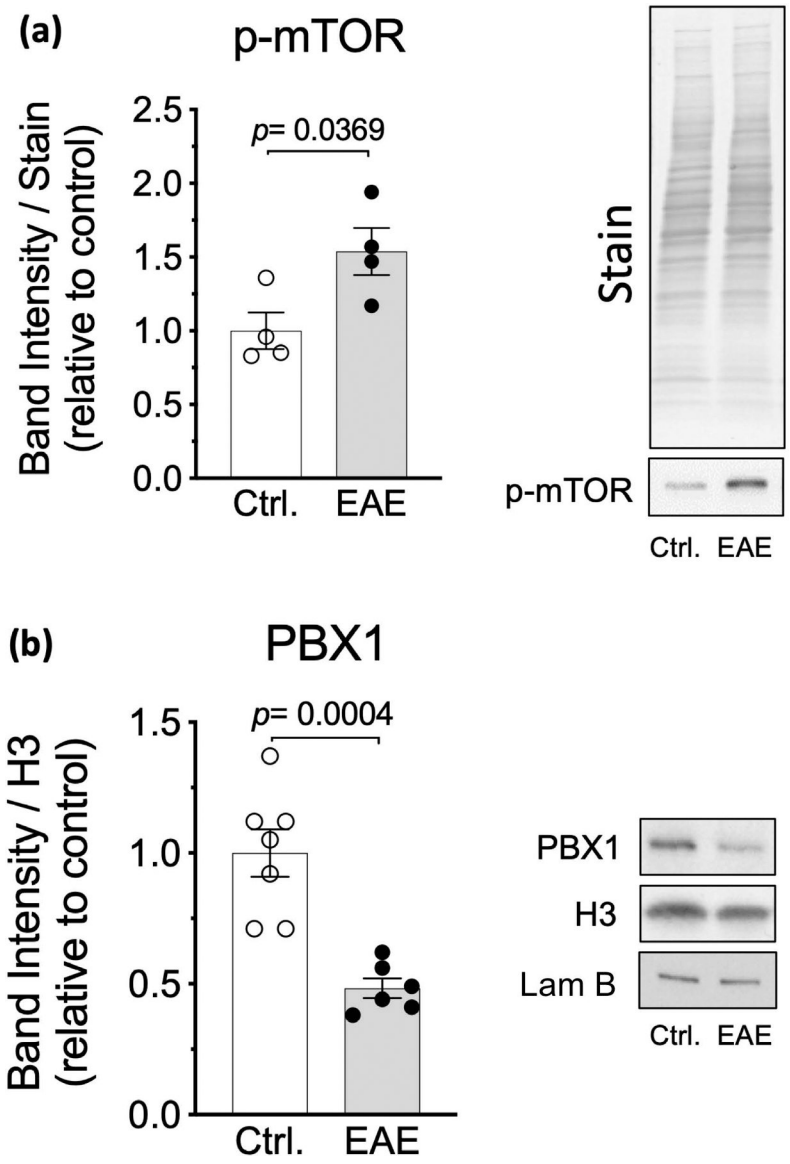

Fig. 10 –.

High levels of p-mTOR and reduced expression of PBX1 in EAE. **(a)** The amount of p-mTOR in spinal cord homogenates from control and EAE mice at 30 dpi was determined by western blot analysis. Band intensities were corrected by the amount of Coomassie blue staining in the same gel lanes. **(b)** PBX1 levels in the nuclear fractions from control and EAE spinal cords at 30 dpi were determined by western blot analysis. Band intensities were corrected by the amount of histone H3 in the same gel lanes. In both panels, each point represents one animal. Values are expressed relative to controls. Bars and horizontal lines depict the mean ± SEM of 4–7 animals. Statistical significance was determined by Student's *t*-test. Lam B, lamin B1.

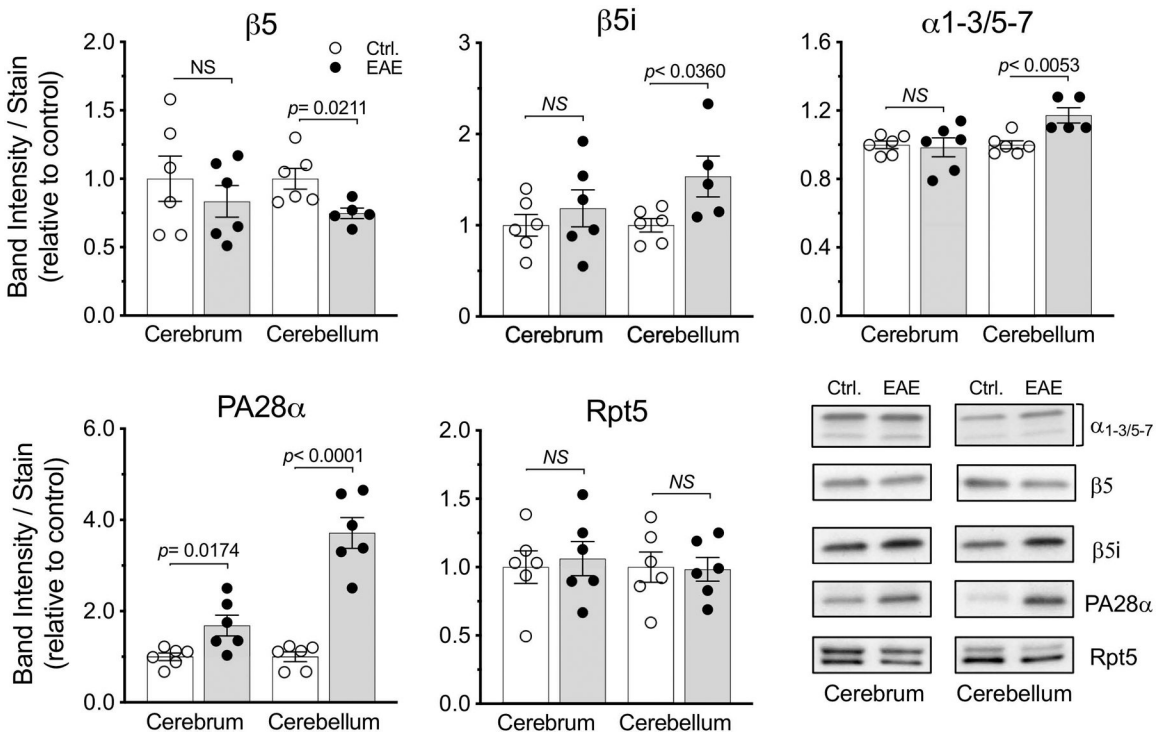

Fig. 11 –.

Altered proteasome composition in the cerebella, but not the cerebra, of EAE mice. Levels of subunits β5, β5i, α1–3/5–7, PA28α and Rpt5 in the cerebra and cerebella of control and EAE mice at 30 dpi were determined by western blot analysis. Band intensities were corrected by the amount of Coomassie blue staining in the same gel lanes. Each point represents one animal. Values are expressed relative to controls. Bars and horizontal lines depict the mean ± SEM of 5–6 animals. Statistical significance was determined by Student's *t*-test. *NS*, not significant. Lower right panel shows representative western blots of the analyzed subunits.

Table 1–

List of mouse PCR primers used in the study

Proteasome subunits		
Psmb5 / β5	Forward	5’-GATCTGTGGCTGGGATAAGAG-3’
	Reverse	5’-TCCATAACGCCGTAAGCATAC-3’
Psmb8 / β5i	Forward	5’-GCTGCTTTCCAAACATGATGC-3’
	Reverse	5’-CCGAGTCCCATTGTCATCTAC-3’
Psme1 / PA28α	Forward	5’-TCCATCCCGAAGCCCAA-3’
	Reverse	5’-CCTTTAAGAACGCATCCAACTC-3’
Psme2 / PA28β	Forward	5’-TCATATCCCTGAGTCAGCTCT-3’
	Reverse	5’-TGCTTGTCTGTTTCCATCTCG-3’
Psmc3 / Rpt5	Forward	5’-GATCATACCCGCCTCCAC-3’
	Reverse	5’-ATCATGCAGATCCACTCACG-3’
Psma7 / α7	Forward	5’-ACAATGTCCTTTCCTCGAACA-3’
	Reverse	5’-GCCATCACCGTCTTCTCG-3’
Antioxidant Defense		
Nfe2l1 / Nrf-1	Forward	5’-AGCCTTCTATCTCCTCTTCTGA-3’
	Reverse	5’-CTCACTTGCTGATGTATTTACTTCC-3’
Pro-inflammatory cytokines		
Ifng / IFN-γ	Forward	5’-ACGGCACAGTCATTGAAAGC-3’
	Reverse	5’-TCACCATCCTTTTGCCAGTTC-3’
Tnf / TNF-α	Forward	5’-GCCACCTCGCTCTTCTG-3’
	Reverse	5’-TGGTTTGCTACGACGTGGG-3’
Il1b / IL-1β	Forward	5’-GGCTCATCTGGGATCCTCTC-3’
	Reverse	5’-ATCTTTTGGGGTCCGTCAACT-3’
House-keeping genes		
Gapdh / GAPDH	Forward	5’-TGTGATGGGTGTGAACCACGAGAA-3’
	Reverse	5’-GAGCCCTTCCACAATGCCAAAGTT-3’
Hprt1 / HPRT1	Forward	5’-TGGGCTTACCTCACTGCTTT-3’
	Reverse	5’-CTAATCACGACGCTGGGACT-3’
Rplp0 / RPLP0	Forward	5’-TCCAGGCTTTGGGCATCA-3’
	Reverse	5’-CTTTATCAGCTGCACATCACTCAGA-3’
Rn18s / 18S rRNA	Forward	5’-GCAATTATTCCCCATGAACG-3’
	Reverse	5’-GGCCTCACTAAACCATCCAA-3’

Table 2 –

List of primary and secondary antibodies used for western blot analysis.

Primary Antibodies	**Species/Clonality**	**Dilutions**	**Supplier**	**RRID**
20S α1–3/5–7	Mus / mAb	1:500	Enzo Life Science	AB_2052368
20S β5	Rb / pAb	1:2000	Enzo Life Science	AB_2052392
20S β5i	Rb / mAb	1:2000	Cell Signaling Technology	AB_2744693
PA28α	Rb / mAb	1:1000	Abcam	AB_2801483
PA28β	Rb / pAb	1:1000	Abcam	AB_2050212
Rpt5	Rb / mAb	1:2000	Abcam	AB_2801479
Nrf1	Rb / pAb	1:1000	Proteintech	AB_2267298
Histone-H3	Rb / mAb	1:10000	Cell Signaling Technology	AB_10544537
NFκB (p65)	Rb /mAb	1:2000 – 1:5000	Cell Signaling Technology	AB_10859369
IRF-1	Rb / mAb	1:2000	Cell Signaling Technology	AB_10949108
p-mTOR	Rb / mAb	1:2000	Cell Signaling Technology	AB_10691552
p-STAT-1	Rb / mAb	1:2000	Cell Signaling Technology	AB_2773718
PBX1	Rb / pAb	1:2000	Proteintech	AB_10951860
Lamin B1	Mus / mAb	1:5000	Proteintech	AB_2721256
Secondary Antibodies	**Species/Clonality**	**Dilutions**	**Supplier**	**RRID**
Peroxidase-conjugated anti-rabbit IgG	Goat / pAb	1:10,000	Jackson ImmunoResearch	AB_2307391
Peroxidase-conjugated anti-mouse IgG	Goat /pAb	1:10,000	Jackson ImmunoResearch	AB_10015289

Abbreviations: Mus, mouse; Rb, rabbit; mAb, monoclonal antibody; pAb, polyclonal antibody; RRID, research resource identifier.

Table 3 –

List of primary and secondary antibodies used for immunohistochemical analysis.

Primary Antibodies	**Species/Clonality**	**Dilutions**	**Supplier**	**RRID**
20S β5	Rb / pAb	1:100	Enzo Life Science	AB_2052392
20S β5i	Rb / mAb	1:100	Cell Signaling Technology	AB_2744693
PA28β	Rb / pAb	1:50	Abcam	AB_2050212
GFAP	Mus /mAb	1:200	Sigma Aldrich	AB_477010
CAII	Mus /mAb	1:200	Santa Cruz Biotechnology	AB_626796
NeuN	Mus /mAb	1:200	Abcam	AB_2298772
CD45	Rat /mAb	1:25	Life Technology	AB_10372515
Secondary Antibodies	**Species/Clonality**	**Dilutions**	**Supplier**	**RRID**
Cy3-conjugated anti-rabbit IgG	Donkey / pAb	1:500	Jackson ImmunoResearch	AB_2307443
Alexa Fluor 488-conjugated anti-mouse IgG	Goat /F(ab')2	1:500	Thermo-Fisher	AB_143160
Alexa Fluor 488-conjugated anti-rat IgG	Donkey / pAb	1:500	Jackson ImmunoResearch	AB_2340684

Abbreviations: Mus, mouse; Rb, rabbit; mAb, monoclonal antibody; pAb, polyclonal antibody; RRID, research resource identifier.